Interference Characterization in Random Waypoint Mobile Networks

Luis Irio, António Furtado, *Member, IEEE*, Rodolfo Oliveira, *Senior Member, IEEE*, Luis Bernardo, *Member, IEEE*, and Rui Dinis, *Senior Member, IEEE*

***Abstract*— In this paper, we characterize the wireless interference of a mobile ad hoc network, where the nodes move according to the random waypoint model. The interferers are assumed to be located within an interference region that is defined as a circular region centered in a fixed node located at a given point of the mobility scenario. The main contribution of this paper is the characterization of the aggregate interference caused to the fixed node by mobile interferers located within the interference region. The distribution of the interference is analyzed taking into account the stochastic nature of the path loss due to the mobility of the nodes, as well as fast fading and shadowing effects. The derivation of the characteristic function of the aggregate interference is used in two different estimators, which successfully characterize the interference using only a small set of samples. The theoretical approach is validated through simulations, which confirm its effectiveness. Finally, we assess the accuracy of the proposed estimators, demonstrating the practical value of this paper.**

***Index Terms*— Interference modeling, interference estimation, mobile networks, wireless networks.**

I. Introduction

INTERFERENCE plays an important role in the future generation of wireless communication systems because the traditional single transmitter and receiver model is being progressively replaced by a different approach, where multiple nodes may transmit simultaneously for a single or even multiple receivers. This paradigm shift is underway and its advantages are well known [1]. Multiple communication technologies are already implementing this concept, including several examples such as Code Division Multiple Access (CDMA) systems [2], Multi-User Multiple Input Multiple Output (MU-MIMO) [3] and others [4]. In these systems multiple transmitters may act as interferers when a packet transmitted by a specific node is decoded in the receiver. The stochastic nature of the interference due to the multiple fading effects is an important cause of performance degradation. This fact has motivated a plethora of different methods of interference mitigation and characterization, proposed for different networks such as cellular and small cell networks [5], wireless sensor networks [6], [7] and vehicular networks [8].

The characterization of the aggregate interference in wireless networks plays an important role in several applications, ranging from localization [9], [10], security [11], [12], spectrum sensing [13] and others. In the majority of wireless scenarios the characterization of the aggregate interference is a complex task. Although the aggregate interference is often caused by a high number of nodes, and thus the central limit theorem (CLT) applies, most of the times CLT cannot be used due to the existence of dominant interferers [14]. This fact has motivated several authors to characterize the aggregate interference with non-Gaussian models [15]–[17]. While [14]–[18] model the aggregate interference in static networks, the assumption of nodes' mobility introduces a novel degree of uncertainty related with the position of the nodes and their level of mobility.

Mainly due to the complexity of non-Gaussian modeling approaches, aggregate interference modeling in mobile scenarios have received limited attention. As far as we know, the use of statistical information related with the mobility of the interferers in the interference modeling process was only carried out in a few and very recent works [19]–[21]. In [19], the interference is caused by static nodes (cells) and the mobility of the terminals only causes a time-varying displacement with respect to the different cells. The work in [20] considers an *ad hoc* network where the nodes move according to the random direction (RD) model. The Probability Density Function of the distance between any pair of nodes is used to characterize the aggregate interference due to path loss. Since a static receiver is assumed in the RD model, the distances between interferers and the receiving node can be regarded as independent random variables, and the CLT applies. In this case, a Gaussian modeling approach can be used. Reference [21] assumes that interferers may move according to four different mobility models. The random waypoint mobility model (RWP) [22] is adopted in a circular simulation area. The work characterizes the expected interference in the center as well as in the border of the simulation area, the temporal correlation, the outage probability and the outage correlation. While this work does account with all interferers in the

Manuscript received April 20, 2017; revised September 18, 2017, February 2, 2018, and July 25, 2018; accepted August 5, 2018. Date of publication August 28, 2018; date of current version November 9, 2018. This work is funded by FCT through national funds and co-funded by FEDER – PT2020 partnership agreement under the project LISBOA-01-0145-FEDER-030709, project UID/EEA/50008/2013, and grant SFRH/BD/108525/2015. The associate editor coordinating the review of this paper and approving it for publication was R. Zheng. *(Corresponding author: Rodolfo Oliveira.)*

The authors are with the Instituto de Telecomunicações, 1049-001 Lisbon, Portugal, and also with the Departamento de Engenharia Electrotécnica, Faculdade de Ciências e Tecnologia, Universidade Nova de Lisboa, 2829-516 Almada, Portugal (e-mail: l.irio@campus.fct.unl.pt; a.furtado@campus.fct.unl.pt; rado@fct.unl.pt; lflb@fct.unl.pt; rdinis@fct.unl.pt).

Color versions of one or more of the figures in this paper are available online at http://ieeexplore.ieee.org.

Digital Object Identifier 10.1109/TWC.2018.2866426

expectation of the aggregate interference, it only considers the contribution of the nearest interferer in the distribution of the interference caused to a node positioned at the center of the simulation area.

Recently, a novel non-Gaussian modeling approach was presented in [23] for the aggregate interference sensed in a fixed point of the network, when the interferers move according to the RWP model. Using the spatial distribution of the nodes moving according to the RWP model, which was characterized in [24] and [23] characterizes aggregate interference due to the path loss effect caused by the multiple moving nodes.

This work extends our work in [23], and has the following contributions:

- Differently from [23], which only considers the path loss effect, in this work we consider both path loss, shadowing/slow fading and fast fading. While it can be understood as a minor contribution when compared to [23], we highlight that the assumption of shadowing/slow fading and fast fading changes the distribution of the power received from each interferer, which impacts on the derivation of the Moment Generating Function of the aggregate interference. In this way, its impact in the aggregate interference model is not marginal, as demonstrated in this work;
- While Poisson point processes have been considered so far to model interference in wireless networks, in several scenarios the Poisson process describing the interferers' location is not homogeneous. Recently, [25] proposed new tools that allow the calculation of a class of functionals on Poisson point processes, including Inhomogeneous Poisson processes. Inhomogeneous Poisson processes were also considered in [26], although not assuming a practical scenario representative of such assumption and not considering mobility. In our work we show that the spatial distribution of the nodes moving according to the RWP mobility model can be represented by an inhomogeneous spatial Poisson process (IPP) [27]. The density of the spatial Poisson process is derived and validated through simulation data, showing that IPP modeling approaches can be adopted in Random Waypoint mobility scenarios simulated in a square/rectangular area;
- By using the IPP, we derive the Moment Generating Function of the aggregate interference when nodes move according to the RWP. The proposed model divides the spatial region where the interferers are located in different regions that are characterized through Poisson processes with different intensities. Shadowing and fast fading propagation effects are considered, which are assumed to be distributed according to a Gamma and a Rayleigh distribution, respectively;
- We provide a theoretical approximation for the aggregate interference distribution of the nodes located within an annulus, and the distribution of the aggregate interference when L annuli are considered. Simulation results validate the interference distribution when path loss, fading and shadowing effects are considered;
- Observing that the aggregate interference can be approximated by a generalized distribution (GEV - Generalized Extreme Value distribution [28]), we adopt a traditional log-likelihood estimator and a probability weighted moments estimator to derive the missing parameters of the distribution. Simulation results show that both estimators achieve high accuracy even for a low number of samples, demonstrating the practical value of this work.

When compared to [21] we highlight that our work addresses a different scenario and the works have different objectives. First of all the focus of our work is the characterization and estimation of the distribution of the aggregate interference at any location of the simulation area. Reference [21] characterizes the expectation of the aggregate interference at the center and at the border of the simulation area and is not focused on the distribution of the aggregate interference. Secondly, while we adopt the RWP model in a square/rectangular simulation area, the RWP considered in [21] was simulated in circular area. This fact impacts in the derivation of the distribution, since the spatial distribution of the nodes moving in a square/rectangular simulation area is not circular as in a circular simulation area [29].

In the next section we describe the considered scenario. Section III presents the steps involved to model the distribution of the nodes moving according to the RWP model as an IPP. Section IV describes the steps involved to model the aggregate interference and introduces the estimators adopted in this work. Section V presents simulation results validating the proposed modeling approach and assessing the accuracy of the proposed estimators for different sampling set lengths. Finally, remarks and conclusions are presented in Section VI.

In what follows we use $\mathrm{E}[X]$ to denote the expectation of X, $P(X = x)$ to represent the probability of X, $f_X(x)$ to represent the Probability Density Function (PDF), $F_X(x)$ to represent the Cumulative Distribution Function (CDF), $M_X(s)$ to represent the Moment Generating Function (MGF) and $\varphi_X(t)$ to represent the Characteristic Function (CF).

II. System Description

In this work we consider that nodes move according to the RWP mobility model [22]. In a RWP mobility scenario n nodes move in a region defined by the area $X_{max} \times Y_{max}$. Each node is initially placed in a random position (x, y). The position is sampled from the uniform distributions represented by $x \in [0, X_{max}]$ and $y \in [0, Y_{max}]$. (x, y) represents the starting point. The ending point (x', y') is also uniformly chosen as the starting point (*i.e.* $x' \in [0, X_{max}]$ and $y' \in [0, Y_{max}]$). A node uniformly chooses the velocity $v \in [V_{min}, V_{max}]$ to move from the starting point to the ending point. After reaching the ending point (x', y'), a node remains stopped at the ending point during the pause time, T_p. After elapsing T_p, a node uniformly chooses a new velocity value to move to another ending point uniformly chosen. After reaching the ending point a node repeats the same cycle as many times as required.

Considering that $\mathrm{E}[S]$ represents the expected distance between two random points and $\mathrm{E}[V_{wp}]$ represents the expected velocity of the nodes without considering pause,

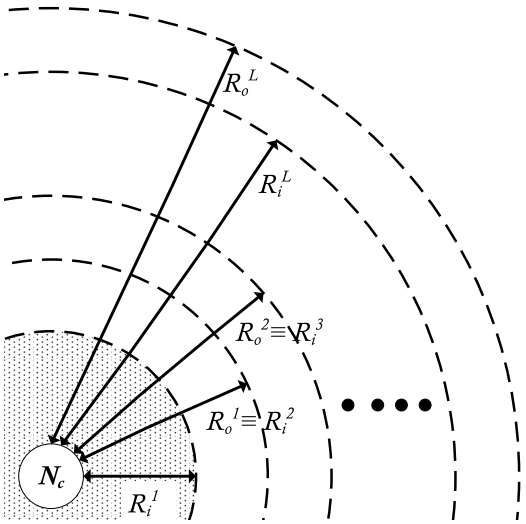

Fig. 1. Aggregate interference caused to N_c due to the hypothetical mobile interferers located in the interference region with area $A = \pi\left((R_o^L)^2 - (R_i^1)^2\right)$.

the expected velocity of the nodes considering pause is given by [24]

$$\mathrm{E}[V] = \left(\frac{\mathrm{E}[S]}{(\mathrm{E}[V_{wp}])^{-1}\mathrm{E}[S] + T_p}\right), \tag{1}$$

where $\mathrm{E}[V_{wp}] = \left(\frac{V_{max}-V_{min}}{\ln\left(\frac{V_{max}}{V_{min}}\right)}\right)$.

The scenario considered in this work is depicted in Figure 1. A fixed node N_c is located at position (x_{N_c}, y_{N_c}), $x_{N_c} \in [0, X_{max}]$ and $y_{N_c} \in [0, Y_{max}]$, which operates as a fixed receiver of the mobile transmitting nodes. The objective of this paper is the characterization of the aggregate interference caused to N_c by the hypothetical transmitters (n) located within the interference region, i.e. the mobile transmitters located in the annulus bounded by the smaller circle of radius R_i^1 and the larger circle of radius R_o^L.

It is assumed that the transmitters access the channel with probability τ.

III. Characterization of the Nodes' Distribution

The area $A = \pi\left((R_o^L)^2 - (R_i^1)^2\right)$ of the annulus in Figure 1 can be obtained via calculus by dividing the annulus up into an infinite number of annuli of infinitesimal width $d\chi$ and area $2\pi\chi\, d\chi$ and then integrating from $\chi = R_i^1$ to $\chi = R_o^L$, i.e. $A = \int_{R_i^1}^{R_o^L} 2\pi\chi\, d\chi$. Using the Riemann sum, A can be approximated by the sum of the area of a finite number (L) of annuli of width ρ,

$$A \approx \sum_{l=1}^{L} A_l, \tag{2}$$

where $A_l = \pi\left((R_o^l)^2 - (R_i^l)^2\right)$ denotes the area of the annulus l. $R_o^l = (R_i^1 + l\rho)$ and $R_i^l = (R_i^1 + (l-1)\rho)$ represent the radius of the larger and smaller circles of the annulus l, respectively.

The number of nodes located in a specific annulus $l \in \{1, ..., L\}$, represented by the random variable (RV) X_l, is approximated by a Poisson process, being its Probability Mass Function (PMF) for a finite domain given by [27]

$$P(X_l = k) = \frac{\frac{(\beta_l A_l \tau)^k}{k!} e^{-\beta_l A_l \tau}}{\sum_{i=0}^{n} \frac{(\beta_l A_l \tau)^i}{i!} e^{-\beta_l A_l \tau}}, k = 0, 1, ..., n, \tag{3}$$

where β_l is the nodes' spatial density in the annulus and n is the total number of mobile nodes.

The spatial PDF of the moving nodes in two dimensions x and y (denoted as $f_{X,Y}(x, y)$) is approximated by (see [24, Th. 3]),

$$f_{XY}(x, y) = (p_s f_{init}(x, y) + p_p(1 - p_s) + (1 - p_s)(1 - p_p) f_m(x, y))/a^2. \tag{4}$$

where $X, Y \in [0, a]$ with $a = X_{max} = Y_{max}$, p_s represents the probability that a node remains static for the entire simulation time, p_p is the probability that a node is resting at a randomly chosen time instant, p_s and $f_{init}(x, y)$ represents the initial spatial node distribution which is a uniform distribution. The probability p_p is given as follows

$$p_p = \frac{(V_{max} - V_{min})T_p}{\ln\left(\frac{V_{max}}{V_{min}}\right)\mathrm{E}[S] + (V_{max} - V_{min})T_p}. \tag{5}$$

The asymptotically stationary PDF of the location of the nodes, $f_m(x, y)$, is given by [24],

$$f_m(x,y) = \begin{cases} f_m^*(x,y) & 0 < x \le \frac{a}{2},\ 0 < y \le x \\ f_m^*(y,x) & 0 < x \le \frac{a}{2},\ x \le y \le \frac{a}{2} \\ f_m^*(a-y,x) & 0 < x \le \frac{a}{2},\ \frac{a}{2} \le y \le a - x \\ f_m^*(x,a-y) & 0 < x \le \frac{a}{2},\ a - x < y \le a \\ f_m^*(a-x,y) & \frac{a}{2} \le x < a,\ 0 < y \le a - x \\ f_m^*(y,a-x) & \frac{a}{2} \le x < a,\ a - x \le y \le \frac{a}{2} \\ f_m^*(a-y,a-x) & \frac{a}{2} \le x < a,\ \frac{a}{2} \le y \le x \\ f_m^*(a-x,a-y) & \frac{a}{2} \le x < a,\ x \le y < a \\ 0, & \text{otherwise,} \end{cases} \tag{6}$$

with

$$f_m^*(x,y) = \frac{6y}{a} + \frac{3}{4}\left(\frac{a^2 - 2ax + 2x^2}{a^2}\right)\left(\frac{y}{y-a} + \frac{y^2}{(x-a)x}\right) + \frac{3y}{2a}\left[\left(\frac{2x}{a} - 1\right)\left(\frac{y}{a} + 1\right)\ln\left(\frac{a-x}{x}\right) + \left(\frac{a^2 - 2ax + 2x^2 + ay}{a^2}\right)\ln\left(\frac{a-y}{y}\right)\right].$$

Knowing the spatial PDF defined in (4), the Bernoulli RV Z_a^l represents the hypothetical location of a node within the

annulus l, and the event of a node being located within the annulus occurs with probability

$$P_l = P(Z_a^l = 1) = \int_{(x_{N_c}-R_o^l)}^{(x_{N_c}+R_o^l)} \int_{\left(y_{N_c}-\sqrt{(R_o^l)^2-(x-x_{N_c})^2}\right)}^{\left(y_{N_c}+\sqrt{(R_o^l)^2-(x-x_{N_c})^2}\right)} f_{XY}(x,y)dydx - \int_{(x_{N_c}-R_i^l)}^{(x_{N_c}+R_i^l)} \int_{\left(y_{N_c}-\sqrt{(R_i^l)^2-(x-x_{N_c})^2}\right)}^{\left(y_{N_c}+\sqrt{(R_i^l)^2-(x-x_{N_c})^2}\right)} f_{XY}(x,y)\,dy\,dx. \quad (7)$$

Consequently, the nodes' spatial density observed in the annulus l, β_l, which is a missing parameter in (3), can be approximated by the expected number of nodes ($n\ P_l$) located in the area A_l, being represented by

$$\beta_l \approx \frac{n\ P_l}{A_l}. \quad (8)$$

More details of the approximation (8) used in the Poisson PMF are given in Appendix A.

At this point, we highlight that the spatial distribution of the nodes ($f_{XY}(x,y)$) brings the specific aspects of the mobility of the nodes into the proposed model. In this way, the specifics of the RWP model and its parameterization are taken into account in $f_{XY}(x,y)$, as described in [24].

Finally, (3) can be used to approximate the distribution of the number of nodes located within each annulus l that approximate the area A. Because the area A may be composed by L areas, representing the area of each annulus l, in what follows we assume that the distribution of the number of nodes located within each annulus l is given by a Poisson process (with PMF represented in (3)). But since the density of nodes within each annulus varies, each annulus has its specific density (β_l). In this way, we approximate the inhomogeneous Poisson process describing the number of nodes in the area A through multiple homogeneous Poisson processes (L) with specific densities.

To validate the proposed methodology, different values of β_l were sampled from several simulations of a mobile scenario parameterized according the data contained in Table I. The mobility of the nodes was simulated during 3000s, which was enough to obtain a spatial distribution of the moving nodes close to the steady state distribution computed with (4). The results collected in 1000 simulations run with different random generator seeds, as well as the numerical results obtained with (8), are illustrated in Figure 2. The x-axis of the figure represents the radial distance from node N_c, which was positioned in the center of the simulated area, i.e. $x_{N_c} = y_{N_c} = 500$m. Three different mobility scenarios were considered. The scenarios were parameterized with the common parameters presented in Table 1 and considering different pause durations (T_p) for each one. An average speed (E[V]) of 10.82m/s was achieved for a pause time $T_p = 0$s, E[V] = 3.52m/s for $T_p = 100$s and E[V] = 1.5m/s for $T_p = 300$s. Each marker in the figure represents the β_l value adopted in each annulus (y-axis), being the width

TABLE I
PARAMETERS ADOPTED IN THE SIMULATIONS

X_{max}	1000 m	Y_{max}	1000 m	Simul. Time	3000 s
V_{min}	5 m/s	V_{max}	20 m/s	τ	1
R_i^1	0 m	ρ	20 m	L	23
n	100	p_s	0	E[S]	$\approx$ 521.4m[24]

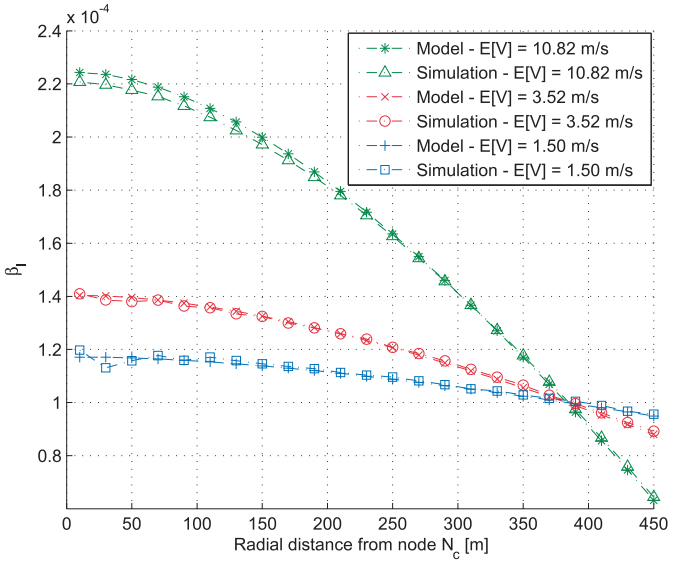

Fig. 2. Validation of β_l for $R_i^1 = 0$ m, $\rho = 20$ m and $L = 23$. The mobility scenario was parameterized according the data in Table I.

of each annulus (ρ) equal to 20m ($R_i^1 = 0$m, $R_o^1 = 20$m, $R_i^2 = 20$m, $R_o^2 = 40$m, etc.). The x-axis represents the radial distance from the transmitter node N_c, being each β_l value represented at the radial distance $R_i^l + \rho/2$. As can be shown, the proposed approximation for β_l in (8) closely follows the results obtained by simulation. Consequently β_l can be used to approximate the intensity of the IPP. Due to the spatial distribution of the nodes, we may observe that β_l decreases as l increases. We can also observe that by increasing T_p the distribution of nodes becomes closer to a uniform distribution (e.g. for E[V] = 1.50m/s the different β_l values become more similar).

The assumption of the nodes being distributed according to a Poisson process within each annulus l was successfully validated. Figure 3 presents the results obtained through simulation and through the PMF in (3) for the mobility scenario considered in Figure 2 when E[V] = 10.82m/s. The β_l values used in (3) were the ones computed and represented in Figure 2 for the same mobility scenario (E[V] = 10.82m/s). Different CDFs are represented for the annulus $l = 2$ ($R_i^2 = 20$m, $R_o^2 = 40$m), $l = 4$ ($R_i^4 = 60$m, $R_o^4 = 80$m), $l = 16$ ($R_i^{16} = 300$m, $R_o^{16} = 320$m) and $l = 23$ ($R_i^{23} = 440$m, $R_o^{23} = 460$m). As can be seen the Poisson distribution accurately approximates the distribution of the number of the nodes within each annulus.

IV. CHARACTERIZATION OF THE AGGREGATE INTERFERENCE

The characterization of the aggregate interference assumes that the interference is sampled periodically.

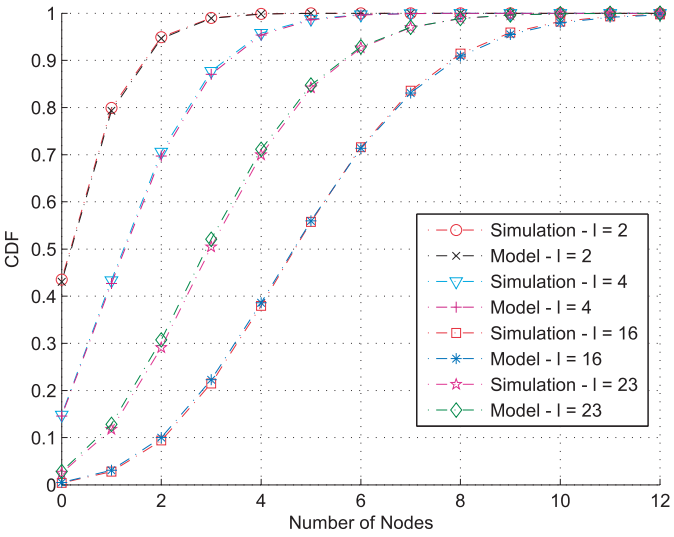

Fig. 3. Validation of $P(X_l \leq k)$ for the mobility scenario $\mathrm{E}[V] = 10.82$m/s considered in Figure 2.

Consequently, different values of mobility of the nodes (e.g. $\mathrm{E}[V]$) lead to different aggregate interference values (e.g. average aggregate interference) when the sampling period is maintained constant. In this Section we start to characterize the interference caused to N_c by the nodes located within a generic annulus l (Subsection IV-A). Then we study the interference caused by the nodes located within L annuli (Subsection IV-B), providing an efficient method to compute the distribution of the aggregate interference (Subsection IV-C). Finally, Subsection IV-D describes the proposed methodologies to estimate the aggregate interference.

A. Interference Due to Interferers Located Within the Annulus l

The total interference power received/sampled by the node N_c located in the center of an annulus l is expressed by

$$I = \sum_{i=1}^{n_l} I_i, \tag{9}$$

where I_i is the interference caused by the i-th node, and n_l is the total number of nodes located in the annulus. The interference power I_i is given by

$$I_i = P_{Tx}\psi_i r_l^{-\alpha} \tag{10}$$

where P_{Tx} is the transmitted power level of the i-th node,[1] ψ_i is an instant value of the fading and shadowing gain observed in the channel between the receiver and node i. r_l represents the distance between the i-th interferer and the receiver. The values r_l and ψ_i represent instant values of the random variables R_l and Ψ_i, respectively. α represents the path-loss coefficient. It should be pointed out that no power control is applied (the generalization for the case with power control is straightforward).

In the next steps we derive the Moment Generating Function of the aggregate interference due to path loss. To characterize the distribution of Ψ_i the small-scale fading (fast fading) and shadowing (slow fading) effects must be considered. The amplitude of the small-scale fading effect is assumed to be distributed according to a Rayleigh distribution, which is represented by

$$f_\zeta(x) = \frac{x}{\sigma_\zeta^2} e^{\frac{-x^2}{2\sigma_\zeta^2}}, \tag{11}$$

where x is the envelope amplitude of the received signal. $2\sigma_\zeta^2$ is the mean power of the multipath received signal. $2\sigma_\zeta^2 = 1$ is adopted in this work to consider the case of normalized power.

Regarding the shadowing effect, we have assumed that its power follows a Lognormal distribution

$$f_\xi(x) = \frac{1}{\sqrt{2\pi}\sigma_\xi x} e^{\frac{-(ln(x)-\mu_\xi)^2}{2\sigma_\xi^2}}, \tag{12}$$

with parameters μ_ξ and σ_ξ. To obtain unitary mean we only parametrize $\sigma_\xi > 0$ and μ_ξ is given by $\mu_\xi = -\frac{\sigma_\xi^2}{2}$.

Although (12) appears to be a simple expression, it is often inconvenient when further analysis are required. Consequently, [30] has shown that the Lognormal distribution can be accurately approximated by a gamma distribution, defined by

$$f_\xi(x) \approx \frac{1}{\Gamma(\vartheta)} \left(\frac{\vartheta}{\omega_s}\right)^{\vartheta} x^{\vartheta-1} e^{-x\frac{\vartheta}{\omega_s}}, \tag{13}$$

where ϑ is equal to $\frac{1}{e^{\sigma_\xi^2}-1}$ and ω_s is equal to $e^{\mu_\xi}\sqrt{\frac{\vartheta+1}{\vartheta}}$. $\Gamma(.)$ represents the Gamma function. The PDF of Ψ_i is thus represented by

$$\begin{aligned} f_{\Psi_i}(x) &\approx f_{\zeta^2}(x) \cdot f_\xi(x) \\ &\approx \frac{2}{\Gamma(\vartheta)} \left(\frac{\vartheta}{\omega_s}\right)^{\frac{\vartheta+1}{2}} x^{\frac{\vartheta-1}{2}} K_{\vartheta-1}\left(\sqrt{\frac{4\vartheta x}{\omega_s}}\right), \end{aligned} \tag{14}$$

which is the Generalized-K distribution, where $K_{\vartheta-1}(\cdot)$ is the modified Bessel function of the second kind.

Due to the analytical difficulties of the Generalized-K distribution, an approximation of the PDF (14) by a more tractable PDF is needed. Reference [31] proposes an approximation of the Generalized-K distribution through a Gamma distribution (the moment matching method was adopted in the approximation). With this method, [31] shows that the scale (θ_ψ) and shape (k_ψ) parameters of the Gamma distribution are given by

$$\theta_\psi = \left(\frac{2(\vartheta+1)}{\vartheta} - 1\right)\omega_s \tag{15}$$

and

$$k_\psi = \frac{1}{\frac{2(\vartheta+1)}{\vartheta} - 1}, \tag{16}$$

respectively.

Let $M_I^i(s)$ represent the MGF of the i-th interferer located within the annulus ($i = 1, ..., n_l$) given by

$$M_I^i(s) = \mathrm{E}_{I_i}[e^{sI_i}] = \mathrm{E}_{\Psi_i}\left[\mathrm{E}_{R_l}[e^{sI_i}]\right]. \tag{17}$$

[1] $P_{Tx} = 10^3$mW is assumed for each node.

The PDF of R_l can be written as the ratio between the perimeter of the circle with radius x and the total area A_l, being represented as follows

$$f_{R_l}(x) = \begin{cases} \dfrac{2\pi x}{A_l} & R_i^l < x < R_o^l. \\ 0, & otherwise \end{cases} \tag{18}$$

Using the PDF of the distance given in (18) and the PDF of the small-scale fading and shadowing effects in (14), the MGF of the interference received by the node N_c due to the i-th interferer node in (17) can be written as follows

$$M_I^i(s) = \int_0^{+\infty} \int_{R_i^l}^{R_o^l} e^{sI_i} f_{R_l}(r_l) f_{\Psi_i}(\psi_i)\, dr_l\, d\psi_i, \tag{19}$$

which using (10), (15), (16), and (18) can be simplified to

$$M_I^i(s) = \frac{2\pi}{A_l(2+k_\psi\alpha)(P_{Tx}\theta_\psi s)^{k_\psi}} \cdot \left(\left(R_o^l\right)^{2+k_\psi\alpha} \varrho(R_o^l) - \left(R_i^l\right)^{2+k_\psi\alpha} \varrho(R_i^l) \right), \tag{20}$$

where

$$\varrho(x) = {}_2\mathrm{F}_1\left(k_\psi, k_\psi + \frac{2}{\alpha}, 1 + k_\psi + \frac{2}{\alpha}, -\frac{x^\alpha}{P_{Tx}\theta_\psi s}\right),$$

and ${}_2\mathrm{F}_1$ represents the Gauss Hypergeometric function [32].

Assuming that the individual interference I_i is independent and identically distributed when compared to the other interferers, the PDF of the aggregate interference I given a total of k active interferers is the convolution of the PDFs of each I_i. Following this rationale, the MGF of I is given by

$$M_{I/k}(s) = M_I^1(s) \times M_I^2(s) \times \cdots\cdots \times M_I^k(s) = \left(M_I^i(s)\right)^k. \tag{21}$$

Using the law of total probability, the PDF of the interference I can be written as

$$f_I(j) = \sum_{k=0}^{n} f_I(j|X_l = k)\mathrm{P}(X_l = k), \tag{22}$$

leading to the MGF of the aggregate interference, I, which can be written as

$$\begin{aligned} \mathrm{E}[e^{sI}] &= \sum_{k=0}^{n} \mathrm{P}(X_l = k) \int_{-\infty}^{+\infty} e^{sj} f_I(j|X_l = k)\, dj \\ &= \sum_{k=0}^{n} \mathrm{P}(X_l = k) M_{I/k}(s). \end{aligned} \tag{23}$$

Using (21), the MGF of I is given as follows

$$\mathrm{E}[e^{sI}] = \sum_{k=0}^{n} \mathrm{P}(X_l = k) e^{k\, ln(M_I^i(s))}. \tag{24}$$

Using the MGF of the Poisson distribution in (24), the MGF of I is finally given by

$$\mathrm{E}[e^{sI}] = e^{\beta_l A_l \tau (M_I^i(s) - 1)}. \tag{25}$$

The first- and second-order statistics of the aggregate interference caused to N_c by the nodes located within the annulus l are an important feature. $\mathrm{E}[I]$, the expected value of the aggregate interference, can be determined by using the Law of Total Expectation. It can be shown that

$$\begin{aligned} \mathrm{E}[I] &= \mathrm{E}\Big[\mathrm{E}\big[I|X_l\big]\Big] = \mathrm{E}\big[I_i\big]\mathrm{E}\big[X_l\big] \\ &= 2\pi\beta_l\tau P_{Tx} e^{\mu_\xi} \sqrt{e^{\sigma_\xi^2}} \left(\frac{(R_o^l)^{2-\alpha} - (R_i^l)^{2-\alpha}}{2-\alpha} \right). \end{aligned} \tag{26}$$

Making similar use of the Law of Total Variance, the variance of the aggregate interference can be described as

$$\mathrm{Var}[I] = \mathrm{Var}[I_i]\mathrm{E}[X_l] + \mathrm{E}[I_i]^2\mathrm{Var}[X_l]. \tag{27}$$

Since X_l is given by a Poisson distribution (with mean and variance $\beta_l A_l \tau$), the variance of the aggregate interference is given as follows

$$\begin{aligned} \mathrm{Var}[I] &= \beta_l A_l \tau \left(\frac{\partial^2 M_I^i(0)}{\partial s^2} \right) \\ &= \pi\beta_l\tau P_{Tx}^2 k_\psi \theta_\psi^2 (1+k_\psi) \left(\frac{(R_o^l)^{2-2\alpha} - (R_i^l)^{2-2\alpha}}{1-\alpha} \right). \end{aligned} \tag{28}$$

The first and second moments can be matched with the respective moments of a given distribution to obtain an approximation of the aggregate interference. As shown in [26], the aggregate interference due to path loss, fast fading and shadowing effect can be approximated by a Gamma distribution. Consequently, the shape and the scale parameters of the Gamma distribution, denoted by k_l and θ_l, are respectively given by

$$k_l = \mathrm{E}[I]^2/\mathrm{Var}[I], \tag{29}$$

and

$$\theta_l = \mathrm{Var}[I]/\mathrm{E}[I]. \tag{30}$$

B. Interference Due to Interferers Located Within L Annuli

As shown before, the interference I caused by interferers located within the l-th annulus is approximated by a gamma distribution, with MGF

$$M_{I/K}^l(s) = (1 - \theta_l s)^{-k_l}. \tag{31}$$

Since the annulus of width $R_o^L - R_i^1$ where the interferers are located can be expressed as a summation of L annuli of width ρ, the MGF of the aggregate interference caused by the interferers located within the L annuli is given by

$$M_{I_{agg}}(s) = \prod_{l=1}^{L} (1 - \theta_l s)^{-k_l}. \tag{32}$$

Finally, the expectation of the aggregate interference can be computed as follows

$$\mathrm{E}[I_{agg}] = \frac{\partial M_{I_{agg}}(0)}{\partial s}. \tag{33}$$

C. Distribution of the Aggregate Interference

The aggregate interference may be stated as being the summation of the L individual aggregated interference caused by the nodes located within each annulus. Expressions for the PDF and the CDF of the summation of L independent gamma random variables were initially derived by Mathai [33]. Those were simplified in [34] in order to be computed more efficiently.

Let $\{Z_l\}_{l=1}^{L}$ be independent but not necessarily identically distributed gamma variables with parameters k_l (shape) and θ_l (scale). The PDF of the aggregate interference is written as $I_{agg} = \sum_{l=1}^{L} Z_l$, which can be approximated by [34]

$$f_{I_{agg}}(x) \approx \prod_{l=1}^{L} \left(\frac{\theta_1}{\theta_l}\right)^{k_l} \sum_{w=0}^{+\infty} \frac{\delta_w \; x^{(\sum_{l=1}^{L} k_l + w - 1)} \exp\left(-\frac{x}{\theta_1}\right)}{\theta_1^{(\sum_{l=1}^{L} k_l + w)} \; \Gamma\left(\sum_{l=1}^{L} k_l + w\right)}, \tag{34}$$

where $\theta_1 = \min_l\{\theta_l\}$, δ_w coefficients are computed recursively,

$$\delta_{w+1} = \frac{1}{w+1} \sum_{i=1}^{w+1} \left[\sum_{l=1}^{L} k_l \left(1 - \frac{\theta_1}{\theta_l}\right)^i\right] \delta_{w+1-i},$$

and $\delta_0 = 1$. $\Gamma(.)$ is the gamma function. Finally, the CDF of I_{agg}, $F_{I_{agg}}(x) = \int_{-\infty}^{x} f_{I_{agg}}(z)dz$, is computed as follows [34]

$$F_{I_{agg}}(x) \approx \prod_{l=1}^{L} \left(\frac{\theta_1}{\theta_l}\right)^{k_l} \sum_{w=0}^{\infty} \frac{\delta_w}{\theta_1^{\sum_{l=1}^{L} k_l + w} \; \Gamma\left(\sum_{l=1}^{L} k_l + w\right)} \times \int_{0}^{x} z^{\sum_{l=1}^{L} k_l + w - 1} \exp\left(-\frac{z}{\theta_1}\right) dz. \tag{35}$$

The computation of $f_{I_{agg}}(x)$ and $F_{I_{agg}}(x)$ can also be performed in a more efficient way using the Fast Fourier Transform (FFT) algorithm, instead of using (34) and (35). Since the annulus of width $R_o^L - R_i^1$ where the mobile nodes are located can be described as a sum of L annuli of width ρ, the characteristic function of the aggregate interference (I_{agg}) received from the mobile nodes is given by

$$\varphi_{I_{agg}}(t) = \prod_{l=1}^{L} (1 - \theta_l it)^{-k_l}. \tag{36}$$

Using the Fourier transform, the PDF of the aggregate interference is given as follows,

$$f_{I_{agg}}(x) = \frac{1}{2\pi} \int_{-\infty}^{+\infty} e^{-itx} \varphi_{I_{agg}}(t)dt, \tag{37}$$

which can be numerically calculated using a FFT algorithm. Finally, the CDF of the aggregate interference is given by

$$F_{I_{agg}}(x) = \int_{-\infty}^{x} f_{I_{agg}}(z)dz. \tag{38}$$

D. Interference Estimation

This subsection starts from the assumption that the aggregate interference can be approximated by a GEV (Generalized Extreme Value) distribution [28]. This assumption was based on sample data obtained through simulation, which was used in different goodness of fit tests to identify the theoretical distributions that better approximate the empirical distribution of the sample data. The results presented in Section V validate our assumption and show the accuracy of the approximation.

The PDF of a GEV distribution is represented by

$$f(x; \sigma, \gamma, \mu) = \frac{1}{\sigma} t(x)^{\gamma+1} e^{-t(x)}, \tag{39}$$

where

$$t(x) = \begin{cases} \left(1 + \gamma \frac{x-\mu}{\sigma}\right)^{-1/\gamma}, & \gamma \neq 0 \\ e^{-(x-\mu)/\sigma}, & \gamma = 0. \end{cases} \tag{40}$$

With the help of two estimators we plan to estimate the parameters σ, γ and μ of the GEV distribution. To this end, a Maximum Log-likelihood estimator (MLE) and a Probability Weighted Moments (PWM) estimator are introduced next, in order to be used in real-time to estimate the aggregate interference. Hereafter, we represent the interference sample set by $\mathcal{X} = \{S_1, S_2, ..., S_m\}$, where $S_1, S_2, ..., S_m$ are the samples periodically acquired by the node N_c. The ordered sample set is denoted by $\mathcal{X}_s = \{S_{1,m}, S_{2,m}, ..., S_{m,m}\}$, where $S_{1,m} \leq S_{2,m} \leq ... \leq S_{m,m}$.

1) MLE: The log-likelihood function for a sample set $\mathcal{X} = \{S_1, ..., S_m\}$ of i.i.d. GEV random variables is given by

$$\log L(\sigma, \gamma, \mu) = -m \log \sigma - \left(\frac{1}{\gamma} + 1\right) \sum_{i=1}^{m} \log\left(1 + \gamma \frac{S_i - \mu}{\sigma}\right) - \sum_{i=1}^{m} \log\left(1 + \gamma \frac{S_i - \mu}{\sigma}\right)^{-1/\gamma}, \tag{41}$$

under the condition $1 + \gamma \frac{S_i - \mu}{\sigma} > 0$. The MLE estimator $(\hat{\sigma}, \hat{\gamma}, \hat{\mu})$ for (σ, γ, μ) is obtained by maximizing (41).

2) PWM Estimator: As described in [35], the PWM of a random variable X with distribution function $F(X) = P(X \leq x)$ are the quantities

$$M_{p,r,s} = \mathrm{E}[X^p (F(X))^r (1 - F(X))^s], \tag{42}$$

for real p, r and s values. For the GEV distribution, [36] shows that $\mathrm{E}[X(F(X))^r]$ can be written as

$$M_{1,r,0} = \frac{1}{r+1} \left\{\mu - \frac{\sigma}{\gamma}[1 - (r+1)^{\gamma} \Gamma(1 - \gamma)]\right\}, \tag{43}$$

with $\gamma < 1$ and $\gamma \neq 0$. The PMW estimators $(\hat{\sigma}, \hat{\gamma}, \hat{\mu})$ of the GEV parameters (σ, γ, μ) are the solution of the following system of equations

$$\begin{cases} M_{1,0,0} = \mu - \frac{\sigma}{\gamma}(1 - \Gamma(1 - \gamma)) \\ 2M_{1,1,0} - M_{1,0,0} = \frac{\sigma}{\gamma} \Gamma(1 - \gamma)(2^{\gamma} - 1) \\ \frac{3M_{1,2,0} - M_{1,0,0}}{2M_{1,1,0} - M_{1,0,0}} = \frac{3^{\gamma} - 1}{2^{\gamma} - 1}, \end{cases} \tag{44}$$

TABLE II
PARAMETERS ADOPTED IN THE SIMULATIONS

X_{max}	1000m	Y_{max}	1000m	p_s	0s
V_{min}	5m/s	V_{max}	20m/s	τ	1
R_i^1	20m	ρ	20m	L	5
Simulation time	3000 s	α	2	σ_ξ	0.69

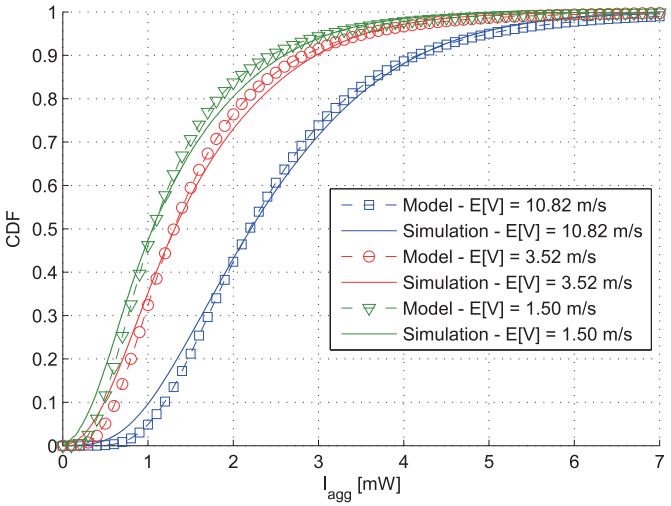

Fig. 4. CDF of the aggregate interference considering the path loss effect ($\tau = 1$).

in which $M_{1,r,0}$ can be replaced by the unbiased estimator proposed in [37]

$$\hat{M}_{1,r,0} = \frac{1}{m}\sum_{j=1}^{m}\left(\prod_{l=1}^{r}\frac{j-l}{m-l}\right)S_{j,m}. \tag{45}$$

V. MODEL EVALUATION

Several simulations were parameterized according the data in Table II to validate the average aggregate interference. A mobility region consisting of a square area of 1000x1000m was defined where the nodes move with $V_{min} = 5$m/s and $V_{max} = 20$m/s. Different mobility scenarios were considered: an average speed (E$[V]$) of 10.82m/s was achieved for a pause time $T_p = 0$s; a second scenario was defined with E$[V] = 3.52$m/s adopting $T_p = 100$s; and a third scenario was defined to obtain E$[V] = 1.5$m/s considering $T_p = 300$s. The aggregate interference was sampled every second and 3×10^6 simulations were run.

To evaluate the proposed model of the aggregate interference we compare the numerical results obtained with the model and the results obtained through simulation. The CDF of the aggregate interference is illustrated in Figure 4 and Figure 5 for a simulation scenario considering $n = 100$ mobile nodes. The receiver node N_c was positioned in the center of the simulation area, i.e. $x_{N_c} = y_{N_c} = 500$m. The aggregate interference was measured by the node N_c every second. In Figure 4 only the path loss effect was considered, while the results plotted in Figure 5 were obtained considering path loss, fast fading and shadowing effect, for $\sigma_\xi = 0.69$. The numerical results were obtained with (35)

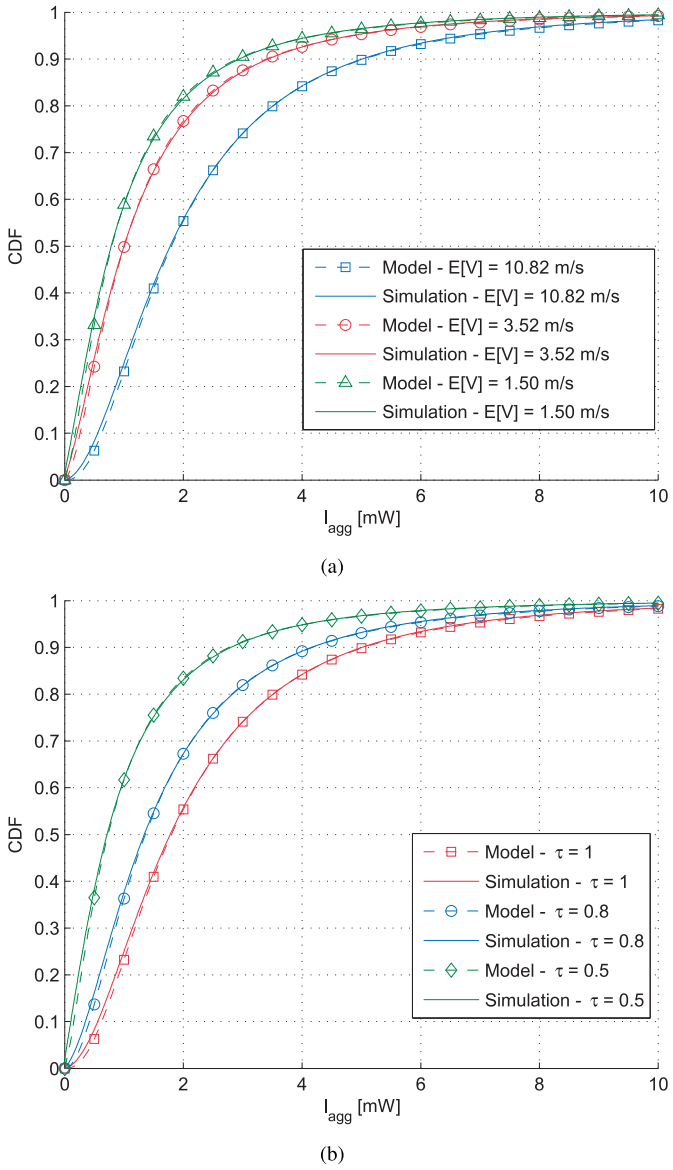

Fig. 5. CDF of the aggregate interference considering path loss, small-scale fading and shadowing effect ($\sigma_\xi = 0.69$): (a) for $\tau = 1$ and E$[V] = \{1.5, 3.52, 10.82\}$m/s; (b) for $\tau = \{0.5, 0.8, 1\}$ and E$[V] = 10.82$m/s.

considering the first 25 terms in the infinite sum series, i.e, $w = 25$.

As shown in both Figures 4 and 5, the error observed between the model and the simulations is in range with the error bound given in [34] for the case when the approximation in (35) is adopted. Different CDFs are obtained for the three mobility scenarios (E$[V]$ =10.82m/s, E$[V]$ = 3.52m/s and E$[V]$ = 1.5m/s), indicating that an increase of T_p leads to a decrease of the aggregate interference power, or in other words, the interference power increases with the average speed of the nodes. This fact is due to the decrease of the node's density near to the node N_c as T_p increases, which is also confirmed by the theoretical analysis in [24] and the values of β_l represented in Figure 2. As the average pause time increases, the spatial distribution of the nodes converges to a uniform distribution, and a smaller number of nodes is located in the vicinity of N_c, causing less interference

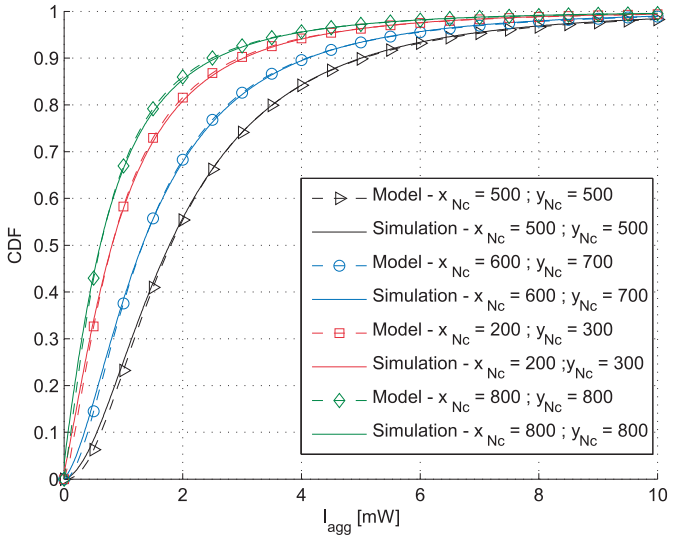

Fig. 6. CDF of the aggregate interference for different positions (x_{Nc}, y_{Nc}) of the receiver node N_c.

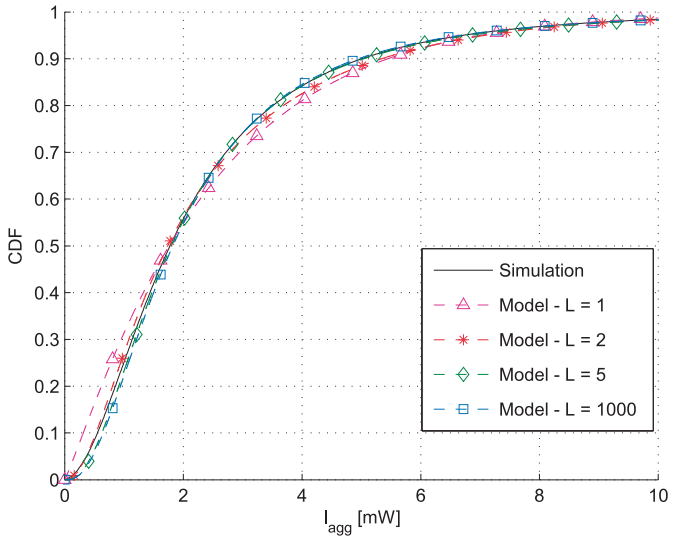

Fig. 7. CDF of the aggregate interference considering path loss, small-scale fading and shadowing effect ($\sigma_\xi = 0.69$), for $L = \{1, 2, 5, 1000\}$, $\mathrm{E}[V] = 10.82$m/s, $\tau = 1$ and $x_{N_c} = y_{N_c} = 500$m.

to N_c. Contrarily, the increase of the mobility increases the average number of nodes in the vicinity of N_c, causing more interference to N_c.

Comparing the results plotted in Figures 4 and 5(a), we observe that when small-scale fading and shadowing are considered, the average interference power remains approximately the same because small-scale fading and shadowing are parametrized for unitary mean.

The proposed model can handle the case when nodes transmit with a given probability, τ. τ can represent the medium access probability of a specific random MAC protocol (e.g. Slotted Aloha), or even the behavior imposed by fair resource management policies. Different medium access probabilities (τ) were considered in the results presented in Figure 5(b). We have considered the high mobility scenario ($\mathrm{E}[V]$ =10.82m/s) and the same parameters adopted in the results presented in Figure 5(a). The simulations were modified to consider that the interference power received from each mobile node is null when a number randomly (uniformly) generated at each discrete simulation time is above τ. In this way the mobile nodes only contribute to the aggregate interference according to τ. From the validation results, presented in Figure 5(a), we observe that the proposed model also approximates the CDF of the aggregate interference for different τ values. Moreover, the interference power decreases as $\tau \to 0$, as expected.

While the results obtained in Figures 4 and 5 were obtained considering that the receiver node N_c was positioned in the center of the simulation, in Figure 6 we evaluate the accuracy of the proposed model for different positions of N_c. The evaluation was done at positions $(x_{N_c}, y_{N_c}) = \{(200, 300)(500, 500), (600, 700), (800, 800)\}$m. We have considered the high mobility scenario ($\mathrm{E}[V] = 10.82$m/s) and the same parameters adopted in the results presented in Figure 5(a). As can be observed, the results computed with the model are close to the results obtained through simulation. Moreover, we also observe that the aggregate interference decreases as the node N_c is further away from the center of the simulated area ($(x, y) = (500, 500)$m). This is explained by the higher density of mobile nodes in the center of the simulation area, as observed in Figure 2. Consequently, as N_c is further away from the center of the simulated area less mobile nodes (interferers) are found in the same circular area ($R_i^1 = 20$m and $R_o^L = 120$m).

Figure 7 compares the simulation results with the numerical results obtained for different values of L. Regarding the parameterization of L, both model's accuracy and model's computation time increase with L. However, different simulation results were used to evaluate the accuracy of the model when $L \geq 5$, confirming its effectiveness even for low values of L.

Next, we assess the accuracy of the proposed estimators. Considering the same radio conditions and the two mobility scenarios ($\mathrm{E}[V] = 10.82$m/s and $\mathrm{E}[V] = 1.5$m/s) assumed in Figure 5(a), we computed the CDF of the aggregate interference with the PMW estimator and the MLE. The length of the sample set was $m = 100$. As can be seen in Figure 8, which represents the CDFs obtained by simulation and computed by maximizing (41) (MLE) and solving (44) (PWM), the results achieved with the proposed estimators are close to the results obtained by simulation. In this case the error obtained with the MLE or with the PWM estimator is similar. This fact is mainly due to the length of the sample set (m), as we will see later.

To evaluate the impact of the length of the sample set in the estimation, we have considered the mobility $\mathrm{E}[V] = 10.82$m/s, being the aggregate interference estimated with the PWM estimator considering $m = 50$, $m = 10$, and $m = 5$ samples. The simulation results and the results achieved with the PWM estimator considering the different m values are illustrated in Figure 9. As expected, a larger set of samples allows more accurate results. However, we would like to highlight the quality of the estimation even when a small set of samples

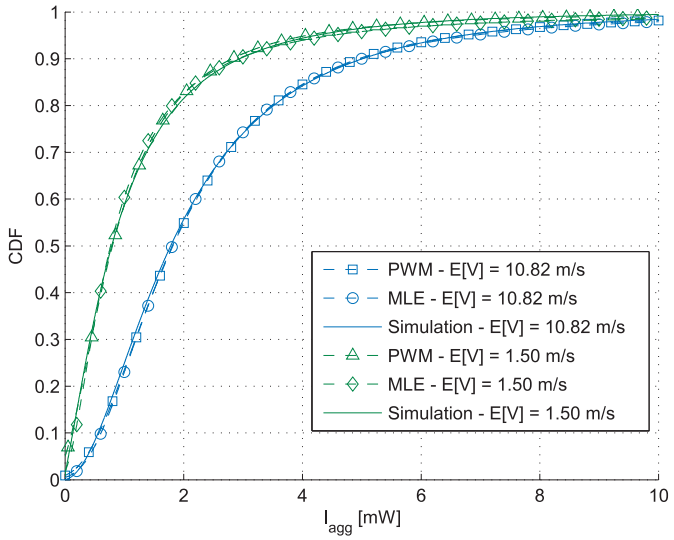

Fig. 8. Estimation of the aggregate interference through the PWM estimator and the MLE (m =100 samples), considering path loss, fading and shadowing effects for two mobility scenarios (E$[V]$ =10.82m/s and E$[V]$ = 1.5m/s, $\tau = 1$).

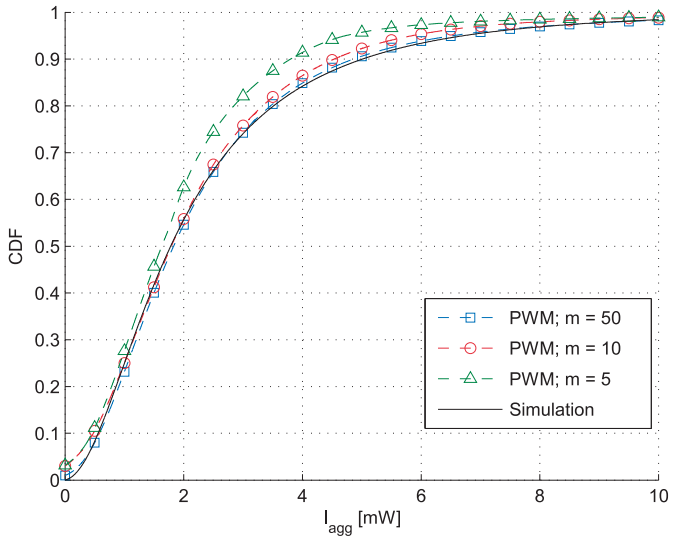

Fig. 9. Estimation of the aggregate interference through the PWM considering different lengths of the sampling set ($m = \{50, 10, 5\}$) for the mobility scenario E$[V]$ =10.82m/s ($\tau = 1$).

($m = 10$) is adopted. These results confirm the quality of the proposed model and estimator, highlighting the importance to this work in terms of its practical application.

Additionally, we note that the aggregate interference follows a GEV distribution, as confirmed by the estimation results presented in Figures 8 and 9.

As a final remark, although the interferers considered in the results presented in Figures 4, 5, 6, 8 and 9, were always located within an annulus parameterized with $R_i^1 = 20$m and $R_o^L = 120$m, we note that the model (and the estimation methodology) was also successfully validated for other R_i^1 and R_o^L values, including the particular case when all moving nodes are considered, i.e. $R_i^1 = 0$m and $R_o^L \geq \sqrt{(X_{max}/2)^2 + (Y_{max}/2)^2}$ for the cases when N_c is positioned at $x_{N_c} = y_{N_c} = 500$m.

VI. Conclusions

This work characterizes the wireless interference of a mobile *ad hoc* network, when the nodes move according to the Random Waypoint model and considering the path loss, fast fading and shadowing effect. The distribution of the aggregate interference caused to a tagged receiver by moving interferers located within an interference region was characterized. Results from several simulations were compared with the theoretical characterization, showing the accuracy of the proposed methodology. Two different estimators were proposed to characterize the interference. The proposed approach was validated through simulations, confirming its effectiveness and evaluating the accuracy of the proposed estimators even for a small set of samples.

Appendix
Poisson Approximation

This appendix identifies the conditions required to use the Poisson distribution to approximate the number of nodes located within an annulus l.

We start considering an annulus $l \in \{1, ..., L\}$ with area $A_l = \pi\left((R_o^l)^2 - (R_i^l)^2\right)$, where n mobile nodes can be located. The number of nodes located within the annulus l is represented by the random variable X_l. P_l represents the probability of a node being located within the annulus. The Poisson Theorem (PT) in [27, p. 113] states that the Poisson distribution may be used as an approximation of the Binomial distribution, when $P_l \to 0$ and $n \to \infty$, such that the mean value $nP_l = \lambda_l$ remains constant.

Representing the probability of having k nodes located in the annulus l through the Binomial distribution,

$$P(X_l = k) = \binom{n}{k} P_l^k (1 - P_l)^{n-k}, \tag{46}$$

it can be rewritten as

$$P(X_l = k) = \frac{n!}{(n-k)!k!} P_l^k (1 - P_l)^{n-k}. \tag{47}$$

As $n \to \infty$, we know that

$$\frac{n!}{(n-k)!k!} = \frac{n(n-1)...(n-k-1)}{k!} \approx \frac{n^k}{k!}. \tag{48}$$

Assuming that the average number of nodes located in the annulus is given by $\lambda_l = nP_l$, and replacing (48) in (46), we have

$$P(X_l = k) = \frac{\lambda_l^k}{k!}(1 - P_l)^{\frac{\lambda_l}{P_l} - k}. \tag{49}$$

According to PT conditions, $P_l \to 0$. Knowing that

$$\lim_{P_l \to 0} (1 - P_l)^{\frac{1}{P_l}} = e^{-1},$$

(49) can be rewritten as follows,

$$P(X_l = k) = \frac{\lambda_l^k}{k!} e^{-\lambda_l}. \tag{50}$$

Assuming the PT, the Binomial distribution describing the number of nodes within the annulus area may be approximated by the Poisson distribution in (50) (with $\lambda_l = \beta_l A_l$, being

$\beta_l = nP_l/A_l$). We highlight that in the limit conditions (i.e., $n \to \infty$ and $P_l \to 0$), the Poisson distribution can be derived from the binomial one. However, in practical scenarios, the PT conditions must be observed in an approximated way. In our work we have considered a fixed number of nodes (n), and the division of the simulation area in multiple annuli benefits the condition $P_l \to 0$.

REFERENCES

[1] H. R. Sadjadpour, Z. Wang, and J. J. Garcia-Luna-Aceves, "The capacity of wireless ad hoc networks with multi-packet reception," *IEEE Trans. Commun.*, vol. 58, no. 2, pp. 600–610, Feb. 2010.

[2] S. Kishore, L. J. Greenstein, H. V. Poor, and S. C. Schwartz, "Uplink user capacity in a multicell CDMA system with hotspot microcells," *IEEE Trans. Wireless Commun.*, vol. 5, no. 6, pp. 1333–1342, Jun. 2006.

[3] J. Liu, Y. T. Hou, Y. Shi, H. D. Sherali, and S. Kompella, "On the capacity of multiuser MIMO networks with interference," *IEEE Trans. Wireless Commun.*, vol. 7, no. 2, pp. 488–494, Feb. 2008.

[4] A. Rezaee, L. Zeger, and M. Médard, "Multi packet reception and network coding," in *Proc. Mil. Commun. Conf. (MILCOM)*, Oct./Nov. 2010, pp. 1393–1398.

[5] M. Feng, T. Jiang, D. Chen, and S. Mao, "Cooperative small cell networks: High capacity for hotspots with interference mitigation," *IEEE Wireless Commun.*, vol. 21, no. 6, pp. 108–116, Dec. 2014.

[6] C.-S. Sum, H. Harada, F. Kojima, and L. Lu, "An interference management protocol for multiple physical layers in IEEE 802.15.4g smart utility networks," *IEEE Commun. Mag.*, vol. 51, no. 4, pp. 84–91, Apr. 2013.

[7] X. Chang *et al.*, "Accuracy-aware interference modeling and measurement in wireless sensor networks," *IEEE Trans. Mobile Comput.*, vol. 15, no. 2, pp. 278–291, Feb. 2015.

[8] X. Cheng, Q. Yao, M. Wen, C.-X. Wang, L.-Y. Song, and B.-L. Jiao, "Wideband channel modeling and intercarrier interference cancellation for vehicle-to-vehicle communication systems," *IEEE J. Sel. Areas Commun.*, vol. 31, no. 9, pp. 434–448, Sep. 2013.

[9] M. Z. Win *et al.*, "Network localization and navigation via cooperation," *IEEE Commun. Mag.*, vol. 49, no. 5, pp. 56–62, May 2011.

[10] K. Pahlavan, X. Li, and J.-P. Mäkelä, "Indoor geolocation science and technology," *IEEE Commun. Mag.*, vol. 40, no. 2, pp. 112–118, Feb. 2002.

[11] A. Rabbachin, A. Conti, and M. Z. Win, "Wireless network intrinsic secrecy," *IEEE/ACM Trans. Netw.*, vol. 23, no. 1, pp. 56–69, Feb. 2014.

[12] S. Goel and R. Negi, "Guaranteeing secrecy using artificial noise," *IEEE Trans. Wireless Commun.*, vol. 7, no. 6, pp. 2180–2189, Jun. 2008.

[13] A. Rabbachin, T. Q. S. Quek, H. Shin, and M. Z. Win, "Cognitive network interference," *IEEE J. Sel. Areas Commun.*, vol. 29, no. 2, pp. 480–493, Feb. 2011.

[14] M. Chiani, "Analytical distribution of linearly modulated cochannel interferers," *IEEE Trans. Commun.*, vol. 45, no. 1, pp. 73–79, Jan. 1997.

[15] M. Z. Win, P. C. Pinto, and L. A. Shepp, "A mathematical theory of network interference and its applications," *Proc. IEEE*, vol. 97, no. 2, pp. 205–230, Feb. 2009.

[16] P. C. Pinto and M. Z. Win, "Communication in a Poisson field of interferers—Part I: Interference distribution and error probability," *IEEE Trans. Wireless Commun.*, vol. 9, no. 7, pp. 2176–2186, Jul. 2010.

[17] P. C. Pinto and M. Z. Win, "Communication in a Poisson field of interferers—Part II: Channel capacity and interference spectrum," *IEEE Trans. Wireless Commun.*, vol. 9, no. 7, pp. 2187–2195, Jul. 2010.

[18] K. Gulati, R. K. Ganti, J. G. Andrews, B. L. Evans, and S. Srikanteswara, "Characterizing decentralized wireless networks with temporal correlation in the low outage regime," *IEEE Trans. Wireless Commun.*, vol. 11, no. 9, pp. 3112–3125, Sep. 2012.

[19] S. Yarkan, A. Maaref, K. H. Teo, and H. Arslan, "Impact of mobility on the behavior of interference in cellular wireless networks," in *Proc. IEEE Global Telecommun. Conf. (GLOBECOM)*, Nov. 2008, pp. 1–5.

[20] X. Zhang, L. Wu, Y. Zhang, and D. K. Sung, "Interference dynamics in MANETs with a random direction node mobility model," in *Proc. IEEE Wireless Commun. Netw. Conf. (WCNC)*, Apr. 2013, pp. 3788–3793.

[21] Z. Gong and M. Haenggi, "Interference and outage in mobile random networks: Expectation, distribution, and correlation," *IEEE Trans. Mobile Comput.*, vol. 13, no. 2, pp. 337–349, Feb. 2014.

[22] D. B. Johnson and D. A. Maltz, "Dynamic source routing in ad hoc wireless networks," in *Mobile Computing*, vol. 353, T. Imielinski and H. F. Korth, Eds. Norwell, MA, USA: Kluwer, 1996.

[23] L. Irio, R. Oliveira, and L. Bernardo, "Aggregate interference in random waypoint mobile networks," *IEEE Commun. Lett.*, vol. 19, no. 6, pp. 1021–1024, Jun. 2015.

[24] C. Bettstetter, G. Resta, and P. Santi, "The node distribution of the random waypoint mobility model for wireless ad hoc networks," *IEEE Trans. Mobile Comput.*, vol. 2, no. 3, pp. 257–269, Jul. 2003.

[25] U. Schilcher, S. Toumpis, M. Haenggi, A. Crismani, G. Brandner, and C. Bettstetter, "Interference functionals in Poisson networks," *IEEE Trans. Inf. Theory*, vol. 62, no. 1, pp. 370–383, Jan. 2016.

[26] M. Haenggi and R. K. Ganti, "Interference in large wireless networks," *Found. Trends Netw.*, vol. 3, no. 2, pp. 127–248, 2009.

[27] A. Papoulis and S. U. Pillai, *Probability—Random Variables and Stochastic Processes*, 4th ed. New York, NY, USA: McGraw-Hill, 2001.

[28] G. Muraleedharan, C. G. Soares, and C. Lucas, "Characteristic and moment generating functions of generalised extreme value distribution (GEV)," in *Sea Level Rise, Coastal Engineering, Shorelines and Tides*. Commack, NY, USA: Nova, 2011, pp. 269–276.

[29] C. Bettstetter and C. Wagner, "The spatial node distribution of the random waypoint mobility model," in *Proc. Mobile Ad-Hoc Netzwerke, Deutscher Workshop ÜBer Mobile Ad-Hoc Netzwerke (WMAN)*, 2002, pp. 41–58.

[30] A. Abdi and M. Kaveh, "On the utility of gamma PDF in modeling shadow fading (slow fading)," in *Proc. IEEE 49th Veh. Technol. Conf.*, vol. 3, May 1999, pp. 2308–2312.

[31] S. Al-Ahmadi and H. Yanikomeroglu, "On the approximation of the generalized-K distribution by a gamma distribution for modeling composite fading channels," *IEEE Trans. Wireless Commun.*, vol. 9, no. 2, pp. 706–713, Feb. 2010.

[32] M. Abramowitz and I. A. Stegun, *Handbook of Mathematical Functions: With Formulas, Graphs, and Mathematical Tables*. New York, NY, USA: Dover, 1965.

[33] A. M. Mathai, "Storage capacity of a dam with gamma type inputs," *Ann. Inst. Statist. Math.*, vol. 34, no. 1, pp. 591–597, 1982.

[34] P. G. Moschopoulos, "The distribution of the sum of independent Gamma random variables," *Ann. Inst. Statist. Math.*, vol. 37, no. 1, pp. 541–544, 1985.

[35] J. A. Greenwood, J. M. Landwehr, N. C. Matalas, and J. R. Wallis, "Probability weighted moments: Definition and relation to parameters of several distributions expressable in inverse form," *Water Resour. Res.*, vol. 15, no. 5, pp. 1049–1054, 1979.

[36] J. R. M. Hosking, J. R. Wallis, and E. F. Wood, "Estimation of the generalized extreme-value distribution by the method of probability-weighted moments," *Technometrics*, vol. 27, no. 3, pp. 251–261, 1985.

[37] J. M. Landwehr, N. C. Matalas, and J. R. Wallis, "Probability weighted moments compared with some traditional techniques in estimating gumbel parameters and quantiles," *Water Resour. Res.*, vol. 15, no. 5, pp. 1055–1064, 1979.

Luis Irio received the M.Sc. degree in electrical and computer engineering from the Nova University of Lisbon in 2013, where he is currently pursuing the Ph.D. degree in electrical and computer engineering. From 2014 to 2015, he was a Researcher with CTS, Instituto de Desenvolvimento de Novas Tecnologias. He is currently a Researcher with the Instituto de Telecomunicações. His research interests include full-duplex systems, multi-packet reception systems, and wireless mobile systems.

António Furtado (S'12–M'18) received the M.Sc. and Ph.D. degrees in electrical and computer engineering from the Faculdade de Ciências e Tecnologia, Universidade Nova de Lisboa, Portugal, in 2012 and 2018, respectively. In 2013, he joined the Instituto de Desenvolvimento de Novas Tecnologias. He then joined the Instituto de Telecomunicações, where he has been involved in several research projects concerning wireless systems. His main research interests include medium access control protocols for wireless systems, particularly multipacket reception communications systems and cognitive radio networks.

Rodolfo Oliveira (S'04–M'10–SM'15) received the Licenciatura and Ph.D. degrees in electrical engineering from the Faculdade de Ciências e Tecnologia (FCT), Universidade Nova de Lisboa (UNL), Lisbon, in 2000 and 2009, respectively, and the M.Sc. degree in electrical and computer engineering from the Instituto Superior Técnico, Technical University of Lisbon, in 2003. From 2007 to 2008, he was a Visiting Researcher with the University of Thessaly. From 2011 to 2012, he was a Visiting Scholar with Carnegie Mellon University. He is currently an Assistant Professor with the Department of Electrical Engineering, FCT, UNL. He is also a Researcher with the Instituto de Telecomunicações, where he is involved in the areas of wireless communications and networking.

Luis Bernardo (M'03) received the Ph.D. degree from the Instituto Superior Técnico, Technical University of Lisbon, Portugal, in 2002, and the Habilitation degree in telecommunications from the Faculdade de Ciências e Tecnologia (FCT), Universidade Nova de Lisboa (UNL), in 2013. Since 1999, he has been an Assistant Professor with FCT, UNL, where he has been a Researcher with the Departamento de Engenharia Electrotécnica, Instituto de Desenvolvimento de Novas Tecnologias, since 2000. Since 2013, he has been a Researcher with the Instituto de Telecomunicações, Lisbon. His research interests include medium access control protocols for wireless communications, cross-layer optimization of wireless systems, routing protocols, and network modeling.

Rui Dinis (S'96–M'00–SM'14) received the Ph.D. degree from the Instituto Superior Técnico (IST), Technical University of Lisbon, Portugal, in 2001, and the Habilitation degree in telecommunications from Faculdade de Ciências e Tecnologia (FCT), Universidade Nova de Lisboa (UNL), in 2010. From 2001 to 2008, he was a Professor with IST. In 2003, he was an Invited Professor with Carleton University, Ottawa, ON, Canada. He was a Researcher with the Centro de Análise e Processamento de Sinal, IST, from 1992 to 2005, and a Researcher with the Instituto de Sistemas e Robótica from 2005 to 2008. Since 2009, he has been a Researcher with the Instituto de Telecomunicações. He is currently an Associate Professor with FCT, UNL. He has been actively involved in several national and international research projects in the broadband wireless communications area. His research interests include transmission, estimation, and detection techniques. He was an Editor of the IEEE TRANSACTIONS ON COMMUNICATIONS from 2012 to 2017. He was a Guest Editor of *Physical Communication* (Elsevier) (Special Issue on Broadband Single-Carrier Transmission Techniques). He is currently an Editor of the IEEE TRANSACTIONS ON VEHICULAR TECHNOLOGY, the IEEE TRANSACTIONS ON WIRELESS COMMUNICATIONS, and *Physical Communication* (Elsevier).